On an Efficient Finite Element Method for Navier-Stokes-$\overline{\omega}$ with Strong Mass Conservationv

Carolina C. Manica · Monika Neda · Maxim Olshanskii · Leo G. Rebholz · Nicholas E. Wilson

Abstract — We study an efficient finite element method for the NS-$\overline{\omega}$ model, that uses van Cittert approximate deconvolution to improve accuracy and Scott-Vogelius elements to provide pointwise mass conservative solutions and remove the dependence of the (often large) Bernoulli pressure error on the velocity error. We provide a complete numerical analysis of the method, including well-posedness, unconditional stability, and optimal convergence. Additionally, an improved choice of filtering radius (versus the usual choice of the average mesh width) for the scheme is found, by identifying a connection with a scheme for the velocity-vorticity-helicity NSE formulation. Several numerical experiments are given that demonstrate the performance of the scheme, and the improvement offered by the new choice of the filtering radius.

2010 Mathematical subject classification: 76D05; 76F99; 65M60.

Keywords: Navier-Stokes-alpha; Navier-Stokes-omega; approximate deconvolution; Scott-Vogelius elements.

1. Introduction

Recent work on finite element methods (FEM) for the 'α models' of fluid flow has proven their effectiveness at finding accurate solutions to flow problems on coarser spatial and temporal

Carolina C. Manica
Departmento de Matemática Pura e Aplicada, Universidade Federal do Rio Grande do Sul
E-mail: `http://chasqueweb.ufrgs.br/∼carolina.manica`.

Monika Neda
Department of Mathematics, University of Nevada, Las Vegas
E-mail: `Monika.Neda@unlv.edu`.

Maxim Olshanskii
Department of Mechanics and Mathematics, M. V. Lomonosov Moscow State University, Moscow 119899, Russia
E-mail: `Maxim.Olshanskii@mtu-net.ru, http://www.mathcs.emory.edu/∼molshan`.

Leo G. Rebholz
Department of Mathematical Sciences, Clemson University, Clemson, SC 29634
E-mail: `rebholz@clemson.edu, http://www.math.clemson.edu/∼rebholz`.

Nicholas E. Wilson
Department of Mathematical Sciences, Clemson University, Clemson, SC 29634
E-mail: `newilso@clemson.edu`.

discretizations than are necessary for successful direct numerical simulations of the Navier-Stokes equations (NSE) [4, 8, 9, 17, 24, 25, 29, 31, 36]. Of these models, NS-$\overline{\omega}$ stands apart because in addition to its excellent theoretical properties such as well-posedness and energy and model helicity conservation [22, 26], it can be computed efficiently with unconditionally stable algorithms [25]. Hence we restrict attention herein to this model. We study an efficient finite element method for NS-$\overline{\omega}$ together with van Cittert approximate deconvolution to increase accuracy, a natural element choice for the model that provides pointwise mass conservation and removes the effect of the pressure error on the velocity error, and a different approach to choosing the filtering radius parameter that leads to improved results.

With all of the α models, higher formal accuracy to true fluid flow can be achieved if van Cittert approximate deconvolution is used to model the removed fine scales, by deconvolving the filtered terms. Our study of NS-$\overline{\omega}$ includes this type of deconvolution as part of the regularization, giving the continuous model

$$\mathbf{u}_t + (\nabla \times D_N F \mathbf{u}) \times \mathbf{u} + \nabla q - \nu \Delta \mathbf{u} = \mathbf{f}, \tag{1.1}$$
$$\nabla \cdot \mathbf{u} = \mathbf{0}, \tag{1.2}$$

where $\mathbf{u}$ is the velocity field, q the pressure, $\mathbf{f}$ a forcing term, and ν the kinematic viscosity. The function F denotes the Helmholtz filter: $F := (-\alpha^2 \Delta + I)^{-1}$ where $\alpha > 0$ is the filtering radius, and D_N is the Nth order van Cittert approximate deconvolution operator: $D_N := \sum_{n=0}^{N} (I - F)^n$.

The finite element discretization we use for the model (1.1)-(1.2) includes a novel combination of several ideas. The first idea is the linearization of the regularized terms via the method of Baker [1]. This allows for the decoupling of the momentum-mass system from the filtering and deconvolution, thus allowing for the higher orders of deconvolution to be used with minimal effect on computational time, while maintaining unconditional energy stability.

The second idea is the use of the Scott-Vogelius velocity-pressure element pair [38, 39], which is a fundamental component of the scheme. This element choice provides solutions with pointwise conservation of mass and has recently been shown to be LBB stable and admits optimal approximation properties under only mild restrictions [40], provides excellent computational results, and decouples the pressure error from the velocity error, and is easily implemented [6, 7, 27, 28]. Since the goal of NS-$\overline{\omega}$ is to find accurate solutions on coarse meshes, such an element choice will help provide solutions that are more physically plausible; even if particular flow features are captured or an L^2 error comparison against known solution values is small, a solution with poor mass conservation is of little value in most applications. The problem of poor mass conservation for typical finite elements is well known, and choices of (P_2, P_0) elements or discontinuous Galerkin methods are common due to their 'local mass conservation' property, even though such choices have their own sub-optimal features. Another important feature of using Scott-Vogelius element is that it decouples the pressure error from the velocity error, which is important for NS-$\overline{\omega}$. Since NS-$\overline{\omega}$ is a rotational form model, its pressure approximates Bernoulli pressure, and is thus more complex than usual pressure and susceptible to large error, especially near walls [23, 31, 32, 33]. This element choice keeps the pressure error from adversely affecting the velocity error.

Lastly, we offer a different approach to choosing the filtering radius α, based on a connection between the model's discretization and a splitting method for the recently proposed velocity-vorticity-helicity (VVH) formulation of the NSE [34]. Error analysis herein and for other α-models has shown that the choice of $\alpha \leqslant O(h)$, where h is the average mesh-width, is

sufficient for optimal asymptotic accuracy [24, 25, 31]. However, on a fixed mesh, the choice $\alpha = ch$ is often used to improve results, where c is a tuning parameter. To aid in this search for a better α, we identify a connection between the NS-$\overline{\omega}$ scheme proposed herein and the VVH splitting method, which suggests a choice of $\alpha = \sqrt{\nu \Delta t}$. Our numerical experiments show that this alternative parameter choice can provide improvement over $\alpha = h$ on some test problems.

This paper is arranged as follows. Section 2 presents notation and preliminaries, and the numerical discretization of NS-$\overline{\omega}$ studied herein. In Section 3, we present a detailed, rigorous analysis of the scheme. We analyze stability and convergence, and the choice of α through the connection to VVH. Compared to the earlier analysis of discretized Navier-Stokes-α models found in [20, 24, 25, 31], in the present paper we are able to remove the time step restriction and to weaken the dependence of constants in error estimate on the Reynolds number (cf. Remark 3.2). Numerical experiments are given in Section 4. Here we demonstrate the improvement in physical fidelity offered by the SV element, provide numerical evidence of the decoupling of the velocity error from the pressure error for SV element solutions (and not for Taylor-Hood (TH) element solutions), and other numerical experiments which show that the proposed method is able to obtain accurate answers on benchmark problems.

2. Preliminaries

This section summarizes the notation, definitions, and preliminary lemmas needed. We start by introducing the following notation. The $L^2(\Omega)$ norm and inner product will be denoted by $\|\cdot\|$ and $(\cdot, \cdot)$. Likewise, the $L^p(\Omega)$ norms and the Sobolev $W_p^k(\Omega)$ norms are denoted by $\|\cdot\|_{L^p}$ and $\|\cdot\|_{W_p^k}$, respectively. For the semi-norm in $W_p^k(\Omega)$ we use $|\cdot|_{W_p^k}$. H^k is used to represent the Sobolev space $W_2^k(\Omega)$, and $\|\cdot\|_k$ denotes the norm in H^k. For functions $v(x,t)$ defined on the entire time interval $(0, T)$, we define $(1 \leqslant m < \infty)$

$$\|v\|_{\infty,k} := \operatorname*{ess\,sup}_{0 < t < T} \|v(t, \cdot)\|_k, \qquad \text{and} \qquad \|v\|_{m,k} := \left(\int_0^T \|v(t, \cdot)\|_k^m \, dt \right)^{1/m}.$$

In the discrete case, we use the analogous norms

$$\|\!|v|\!\|_{\infty,k} := \max_{0 \leqslant n \leqslant M} \|v_n\|_k, \qquad \|\!|v_{1/2}|\!\|_{\infty,k} := \max_{0 \leqslant n \leqslant M} \|v_{n+1/2}\|_k,$$

$$\|\!|v|\!\|_{m,k} := \left(\sum_{n=0}^M \|v_n\|_k^m \triangle t \right)^{1/m}, \qquad \|\!|v_{1/2}|\!\|_{m,k} := \left(\sum_{n=0}^M \|v_{n+1/2}\|_k^m \triangle t \right)^{1/m}.$$

We will consider the case of internal flow, with Ω being a regular, bounded, polyhedral domain in $\mathbb{R}^d$ ($d = 2$ or 3) and

$$\mathbf{X} = (H_0^1(\Omega))^d := \{\mathbf{v} \in (H^1(\Omega))^d : \mathbf{v}|_{\partial\Omega} = \mathbf{0}\},$$
$$Q = L_0^2(\Omega).$$

We denote the dual space of $\mathbf{X}$ by $\mathbf{X}^*$, with the norm $\|\cdot\|_*$. The space of divergence free functions is denoted

$$\mathbf{V} := \{\mathbf{v} \in \mathbf{X}, (\nabla \cdot \mathbf{v}, q) = 0 \ \ \forall q \in Q\}.$$

We now formally define the conforming finite element spaces, specifically those corresponding to Scott-Vogelius elements, that are subspaces of $\mathbf{X}$ and Q. In space dimension d, we define $\mathbf{X}_h^{SV}$ to be the space of continuous element-wise vector functions of polynomial order $k \geqslant d$ on a mesh $\mathcal{T}_h$,

$$\mathbf{X}_h^{SV} := \{\mathbf{v}_h \in [C^0(\Omega)]^d : \mathbf{v}_{h|T} \in [P_k(T)]^d, \text{ for all } T \in \mathcal{T}_h, \ \mathbf{v}_h = \mathbf{0} \text{ on } \partial\Omega\}.$$

We require that the mesh be built from a barycenter refinement of a regular triangularization (tetrahedralization) of the domain Ω if $k \geqslant d$, but if $k = d-1$ ($k = 2$ in 3D or $k = 1$ in 2D), then a Powell-Sabin mesh must be used, [40, 41].

Note that the velocity space for Scott-Vogelius is the same as for the well-known Taylor-Hood element pair, while the pressure space only differs from Taylor-Hood's in that its pressures are discontinuous, defined by

$$Q_h^{SV} := \{q_h \in L^2(\Omega) : q_{h|T} \in P_{k-1} \text{ for all } T \in \mathcal{T}_h\}.$$

Since it is discontinuous, the dimension of the pressure space for Scott-Vogelius elements is significantly larger than for Taylor-Hood elements. This creates a greater total number of degrees of freedom needed for linear solvers using SV elements, however it is not immediately clear whether this will lead to a significant increase in computational time if specific preconditioners, such as Augmented Lagrangian type are used [2]. Although the velocity spaces of the TH and SV elements are the same, the spaces of discretely divergence free subspaces are different, and thus we denote

$$\mathbf{V}_h^{SV} := \{\mathbf{v}_h \in \mathbf{X}_h^{SV} : (\nabla \cdot \mathbf{v}_h, q_h) = 0 \ \ \forall q_h \in Q_h^{SV}\},$$

which is also the pointwise divergence free subspace of $\mathbf{X}_h^{SV}$. The SV element is very interesting from the mass conservation point of view since its discrete velocity space and its discrete pressure space fulfill an important property, namely

$$\nabla \cdot \mathbf{X}_h^{SV} \subset Q_h^{SV}. \tag{2.1}$$

Thus, using SV elements, weak mass conservation via $(\nabla \cdot \mathbf{v}_h, q_h) = 0, \ \forall q_h \in Q_h^{SV}$ implies strong (pointwise) mass conservation since $\|\nabla \cdot \mathbf{v}_h\| = 0$ by choosing $q_h = \nabla \cdot \mathbf{v}_h$. Such a result, or choice of test function, is not possible with most element choices, including Taylor-Hood.

It was proved by S. Zhang in [40, 41] that the SV elements are LBB stable under these restrictions and admit optimal approximation properties. It is well known that the TH pair is LBB stable for this case and that they satisfy the optimal approximation properties as well, [5, 15]. For the convergence studies, we make use of the following approximation properties:

$$\inf_{\mathbf{v}\in\mathbf{X}_h^{SV}} \|\mathbf{u} - \mathbf{v}\| \ \leqslant \ Ch^{k+1}|\mathbf{u}|_{k+1}, \ \ \mathbf{u} \in (H^{k+1}(\Omega))^d,$$

$$\inf_{\mathbf{v}\in\mathbf{X}_h^{SV}} \|\mathbf{u} - \mathbf{v}\|_1 \ \leqslant \ Ch^{k}|\mathbf{u}|_{k+1}, \ \ \mathbf{u} \in (H^{k+1}(\Omega))^d,$$

$$\inf_{r\in Q_h^{SV}} \|p - r\| \ \leqslant \ Ch^{s+1}|p|_{s+1}, \ \ p \in H^{s+1}(\Omega)$$

Assumption 2.1. *Throughout this report, we will assume that $k \geqslant d$ and that the mesh is created from a barycenter refinement of a regular mesh. Hence, Scott-Vogelius elements are LBB stable and admit optimal approximation properties when used in this report.*

We define a trilinear form and list estimates necessary for the analysis studies.

Definition 2.1. Define $b : \mathbf{X} \times \mathbf{X} \times \mathbf{X} \to \mathbb{R}$, by

$$b(\mathbf{u}, \mathbf{v}, \mathbf{w}) := ((\nabla \times \mathbf{u}) \times \mathbf{v}, \mathbf{w}).$$

Lemma 2.1. *For $\mathbf{u}, \mathbf{v}, \mathbf{w} \in \mathbf{X}$, or $L^\infty(\Omega)$ and $\nabla \times \mathbf{u} \in L^\infty(\Omega)$, when indicated, the trilinear term $b(\mathbf{u}, \mathbf{v}, \mathbf{w})$ satisfies*

$$\begin{align}
|b(\mathbf{u}, \mathbf{v}, \mathbf{w})| &\leqslant \|\nabla \times \mathbf{u}\|\|\mathbf{v}\|_\infty\|\mathbf{w}\|, \tag{2.2}\\
|b(\mathbf{u}, \mathbf{v}, \mathbf{w})| &\leqslant \|\nabla \times \mathbf{u}\|_\infty\|\mathbf{v}\|\|\mathbf{w}\|, \tag{2.3}\\
|b(\mathbf{u}, \mathbf{v}, \mathbf{w})| &\leqslant C_0(\Omega)\|\nabla \times \mathbf{u}\|\|\nabla \mathbf{v}\|\|\nabla \mathbf{w}\|, \tag{2.4}\\
|b(\mathbf{u}, \mathbf{v}, \mathbf{w})| &\leqslant C_0(\Omega)\|\mathbf{v}\|^{1/2}\|\nabla \mathbf{v}\|^{1/2}\|\nabla \times \mathbf{u}\|\|\nabla \mathbf{w}\|, \tag{2.5}
\end{align}$$

and if $\mathbf{u}$, $\mathbf{v}$, $\mathbf{w} \in \mathbf{V}$ and $\mathbf{w} \in (H^2(\Omega))^d$, then

$$|b(\mathbf{u}, \mathbf{v}, \mathbf{w})| \leqslant C\|\mathbf{w}\|_2\|\nabla \mathbf{v}\|\|\mathbf{u}\| \tag{2.6}$$

Proof. The first two estimates follow immediately from the definition of b. The proof of the next two bounds are easily adapted from the usual bounds of the nonlinearity in non-rotational form. The last bound takes more work. Begin with a simple vector identity and that the curl is self-adjoint with $\mathbf{u}$, $\mathbf{v}$, $\mathbf{w} \in \mathbf{X}$

$$|((\nabla \times \mathbf{u}) \times \mathbf{v}, \mathbf{w})| = |(\mathbf{w} \times \mathbf{v}, \nabla \times \mathbf{u})| = |(\nabla \times (\mathbf{w} \times \mathbf{v}), \mathbf{u})| \tag{2.7}$$

Continuing with another vector identity for the curl of the cross of two vectors,

$$\nabla \times (\mathbf{w} \times \mathbf{v}) = \mathbf{v} \cdot \nabla \mathbf{w} - \mathbf{w} \cdot \nabla \mathbf{v} + (\nabla \cdot \mathbf{v})\mathbf{w} - (\nabla \cdot \mathbf{w})\mathbf{v}, \tag{2.8}$$

which reduces since $\mathbf{v}$, $\mathbf{w} \in \mathbf{V}$ to

$$\nabla \times (\mathbf{w} \times \mathbf{v}) = \mathbf{v} \cdot \nabla \mathbf{w} - \mathbf{w} \cdot \nabla \mathbf{v}. \tag{2.9}$$

Combining this with (2.7), we have by Holder and Poincare's inequalities,

$$\begin{align}
|((\nabla \times \mathbf{u}) \times \mathbf{v}, \mathbf{w})| &\leqslant |(\mathbf{v} \cdot \nabla \mathbf{w}, \mathbf{u})| + |(\mathbf{w} \cdot \nabla \mathbf{v}, \mathbf{u})| \\
&\leqslant C\|\mathbf{w}\|_2\|\nabla \mathbf{v}\|\|\mathbf{u}\|. \tag{2.10}
\end{align}$$

$\square$

The error analysis uses a discrete Gronwall inequality, recalled from [16], for example. The specific version given below is given as a remark to Lemma 5.1 in [16].

Lemma 2.2 (Discrete Gronwall Lemma). *Let Δt, H, and a_n, b_n, c_n, d_n (for integers $n \geqslant 0$) be finite nonnegative numbers such that*

$$a_l + \Delta t \sum_{n=0}^{l} b_n \leqslant \Delta t \sum_{n=0}^{l-1} d_n a_n + \Delta t \sum_{n=0}^{l} c_n + H \quad \text{for } l \geqslant 1. \tag{2.11}$$

Then for $\Delta t > 0$

$$a_l + \Delta t \sum_{n=0}^{l} b_n \leqslant \exp\left(\Delta t \sum_{n=0}^{l-1} d_n\right)\left(\Delta t \sum_{n=0}^{l} c_n + H\right) \quad \text{for } l \geqslant 1. \tag{2.12}$$

2.1. Filtering and Deconvolution

Since we study discretizations of a fluid model, we must deal with discrete differential filters. Continuous differential filters were introduced into turbulence modeling by Germano [14] and used for various models and regularizations [3, 10, 17]. They can arise, for example, as approximations to Gaussian filters of high qualitative and quantitative accuracy [13].

Definition 2.2 (Continuous α-filter). For $\mathbf{v} \in (L^2(\Omega))^d$ and $\alpha > 0$ fixed, denote the filtering operation on $\mathbf{v}$ by $\overline{\mathbf{v}}$, where $\overline{\mathbf{v}}$ is the unique solution in $\mathbf{X}$

$$-\alpha^2 \Delta \overline{\mathbf{v}} + \overline{\mathbf{v}} = \mathbf{v}. \tag{2.13}$$

We denote by $F := (-\alpha^2 \Delta + I)^{-1}$, so $F\mathbf{v} = \overline{\mathbf{v}}$. We define next the discrete differential filter following, Manica and Kaya-Merdan [30], but also enforcing incompressibility.

Definition 2.3 (Discrete differential filter). Given $\mathbf{v} \in (L^2(\Omega))^d$, for a given filtering radius $\alpha > 0$, $\overline{\mathbf{v}}^h = F_h \mathbf{v}$ is the unique solution in $\mathbf{X}_h^{SV}$ of: Find $(\overline{\mathbf{v}}^h, \lambda_h) \in (\mathbf{X}_h^{SV}, Q_h^{SV})$ satisfying

$$\alpha^2 (\nabla \overline{\mathbf{v}}^h, \nabla \boldsymbol{\chi}_h) + (\overline{\mathbf{v}}^h, \boldsymbol{\chi}_h) - (\lambda_h, \nabla \cdot \boldsymbol{\chi}_h) + (\nabla \cdot \overline{\mathbf{v}}^h, r_h) = (\mathbf{v}, \boldsymbol{\chi}_h) \quad \forall (\boldsymbol{\chi}_h, r_h) \in (\mathbf{X}_h^{SV}, Q_h^{SV}). \tag{2.14}$$

We now define the van Cittert approximate deconvolution operators.

Definition 2.4. The continuous and discrete van Cittert deconvolution operators D_N and D_N^h are

$$D_N \mathbf{v} := \sum_{n=0}^{N} (I - F)^n \mathbf{v}, \qquad D_N^h \mathbf{v} := \sum_{n=0}^{N} (\Pi_h - F_h)^n \mathbf{v}. \tag{2.15}$$

where Π_h denotes the L^2 projection $\Pi^h : (L^2(\Omega))^d \to \mathbf{X}_h$.

For order of deconvolution $N = 0, 1, 2, 3$ and $\mathbf{v} \in \mathbf{X}_h$ we have

$$\begin{aligned} D_0^h \mathbf{v} &= \mathbf{v}, \\ D_1^h \mathbf{v} &= 2\mathbf{v} - \overline{\mathbf{v}}^h, \\ D_2^h \mathbf{v} &= 3\mathbf{v} - 3\overline{\mathbf{v}}^h + \overline{\overline{\mathbf{v}}^h}^h, \\ D_3^h \mathbf{v} &= 4\mathbf{v} - 6\overline{\mathbf{v}}^h + 4\overline{\overline{\mathbf{v}}^h}^h - \overline{\overline{\overline{\mathbf{v}}^h}^h}^h. \end{aligned}$$

D_N was shown to be an $O(\alpha^{2N+2})$ approximate inverse to the filter operator F in Lemma 2.1 of [11]. The proof is an algebraic identity and holds in the discrete case as well, giving the following.

Lemma 2.3. D_N and D_N^h are bounded, self-adjoint positive operators. For $\mathbf{v} \in (L^2(\Omega))^d$,

$$\mathbf{v} = D_N \overline{\mathbf{v}} + (-1)^{(N+1)} \alpha^{2N+2} \Delta^{N+1} F^{(N+1)} \mathbf{v}$$

and

$$\mathbf{v} = D_N^h \overline{\mathbf{v}}^h + (-1)^{(N+1)} \alpha^{2N+2} \Delta_h^{N+1} F_h^{(N+1)} \mathbf{v}$$

Lemma 2.4. *For $\mathbf{v} \in \mathbf{X}$, we have the following bounds:*

$$\|\overline{\mathbf{v}}^h\| \leqslant \|\mathbf{v}\|, \quad \|\nabla \overline{\mathbf{v}}^h\| \leqslant \|\nabla \mathbf{v}\| \ \ and \ \ \|\nabla \times \overline{\mathbf{v}}^h\| \leqslant \|\nabla \mathbf{v}\|. \tag{2.16}$$

Proof. This proof can be found in [25].

Lemma 2.5. *For $\mathbf{v} \in \mathbf{X}$, we have the following bounds:*

$$\|\nabla \times D_N^h \overline{\mathbf{v}}^h\| \leqslant C(N)\|\nabla \mathbf{v}\|. \tag{2.17}$$

Proof. The proof follows from an inductive argument based on the definition of the deconvolution operator D_N^h and Lemma 2.4.

Lemma 2.6. *For smooth v the discrete approximate deconvolution operator satisfies*

$$\|\mathbf{v} - D_N^h \overline{\mathbf{v}}^h\| \leqslant C\alpha^{2N+2}\|\triangle^{N+1}F^{N+1}\mathbf{v}\| + C(\alpha h^k + h^k)(\sum_{n=1}^{N+1} | F^n \mathbf{v} |_{k+1}). \tag{2.18}$$

The proof is based on using similar arguments as in [24].

The dependence of the $|F^n(\mathbf{v})|_{k+1}$ terms in (2.18) upon the *filter radius* α, for a general smooth function $\boldsymbol{\phi}$, is not fully understood for the case of deconvolution order $N \geqslant 2$ (i.e., for $n \geqslant 2$)[12, 21]. In the case of $\mathbf{v}$ periodic the $|F^n(\mathbf{v})|_{k+1}$ are independent of α. Also, for $\mathbf{v}$ satisfying homogeneous Dirichlet boundary conditions, with the additional property that $\Delta^j \mathbf{v} = 0$ on $\partial\Omega$ for $0 \leqslant j \leqslant \left[\frac{k+1}{2}\right] - 1$, the $|F^n(\mathbf{v})|_{k+1}$ are independent of α. Our analysis of the method is for general N, and thus for $N \geqslant 2$, we make this assumption of independence. However, our computations are for $N = 1$, and our experience has shown that there is typically little or no gain for larger N with polynomials approximating velocities with degree three or less. For elements with higher order polynomials, we would expect a difference.

2.2. A numerical scheme for NS-$\overline{\omega}$

We now are ready to present the NS-$\overline{\omega}$ algorithm we study herein. The scheme uses a trapezoidal temporal discretization, and uses a Baker-type [1] extrapolation to linearize and maintain unconditional stability. We denote $\mathbf{u}(t_{n+1/2}) = \mathbf{u}((t_n + t_{n+1})/2)$ for the continuous variable and $\mathbf{u}^{n+1/2} = (\mathbf{u}^n + \mathbf{u}^{n+1})/2$ for both continuous and discrete variables.

Algorithm 2.1.

Given kinematic viscosity $\nu > 0$, end-time $T > 0$, the time step is chosen $\Delta t < T = M\Delta t$, $\mathbf{f} \in L^\infty(0, T; (H^{-1}(\Omega))^d$, the initial condition $\mathbf{u}_0 \in \mathbf{V}$, the filtering radius $\alpha > 0$, deconvolution order $N \geqslant 0$, first find $\mathbf{u}_h^0 \in \mathbf{X}_h^{SV}$ satisfying

$$(\mathbf{u}_h^0, \mathbf{v}_h) - (\lambda_h, \nabla \cdot \mathbf{v}_h) = (\mathbf{u}_0, \mathbf{v}_h), \quad \forall \mathbf{v}_h \in \mathbf{X}_h^{SV} \tag{2.19}$$

$$(\nabla \cdot \mathbf{u}_h^0, r_h) = 0 \quad \forall r_h \in Q_h^{SV}, \tag{2.20}$$

then set $\mathbf{u}_h^{-1} := \mathbf{u}_h^0$, and find $(\mathbf{u}_h^{n+1}, q_h^{n+\frac{1}{2}}) \in (\mathbf{X}_h^{SV}, Q_h^{SV})$ for $n = 0, 1, ..., M - 1$ satisfying

$$\frac{1}{\Delta t}(\mathbf{u}_h^{n+1} - \mathbf{u}_h^n, \mathbf{v}_h) + ((\nabla \times D_N^h F_h(\frac{3}{2}\mathbf{u}_h^n - \frac{1}{2}\mathbf{u}_h^{n-1}) \times \mathbf{u}_h^{n+\frac{1}{2}}), \mathbf{v}_h)$$

$$- (q_h^{n+\frac{1}{2}}, \nabla \cdot \mathbf{v}_h) + \nu(\nabla \mathbf{u}_h^{n+\frac{1}{2}}, \nabla \mathbf{v}_h) = (\mathbf{f}^{n+\frac{1}{2}}, \mathbf{v}_h) \quad \forall \mathbf{v}_h \in \mathbf{X}_h^{SV}, \tag{2.21}$$

$$(\nabla \cdot \mathbf{u}_h^{n+1}, r_h) = 0 \quad \forall r_h \in Q_h^{SV}. \tag{2.22}$$

3. Analysis of the scheme

In this section, we show that solutions of the NS-$\overline{\omega}$ algorithm are unconditionally energy-stable, i.e., discrete solutions obey the energy estimate and are optimally convergent. Since NS-$\overline{\omega}$ approximates NSE solutions, we study the convergence analysis of the finite element solutions of NS-$\overline{\omega}$ to the true solutions of the NSE.

We shall assume that the solution to the NSE that is approximated by the model is a strong solution and, in particular, satisfies $\mathbf{w} \in L^2(0,T;X) \cap L^\infty(0,T;(L^2(\Omega))^d) \cap L^4(0,T;X)$, $p \in L^2(0,T;Q)$, $\mathbf{w}_t \in L^2(0,T;X^*)$ and

$$(\mathbf{w}_t, \mathbf{v}) + b(\mathbf{w}, \mathbf{w}, \mathbf{v}) - (p, \nabla \cdot \mathbf{v}) + \nu(\nabla \mathbf{w}, \nabla \mathbf{v}) \; = \; (\mathbf{f}, \mathbf{v}) \quad \forall \mathbf{v} \in X, \qquad (3.1)$$

$$(q, \nabla \cdot \mathbf{w}) \; = \; 0 \quad \forall q \in Q. \qquad (3.2)$$

3.1. Stability and well-posedness

Lemma 3.1. *Consider the NS-$\overline{\omega}$ algorithm 2.1. A solution $\mathbf{u}_h^l$, $l = 1, \ldots M$, exists at each time-step and it is unique. The algorithm is also unconditionally energy-stable: the solutions satisfy the á priori bound*

$$\|\mathbf{u}_h^M\|^2 + \nu \Delta t \sum_{n=0}^{M-1} \|\nabla \mathbf{u}_h^{n+1/2}\|^2 \leqslant \|\mathbf{u}_h^0\|^2 + \frac{\Delta t}{\nu} \sum_{n=0}^{M-1} \|\mathbf{f}^{n+1/2}\|_*^2. \qquad (3.3)$$

Proof. The á priori bound can be obtained by setting $\mathbf{v}_h = \mathbf{u}_h^{n+1/2}$ in (2.21). The nonlinear term in the scheme vanishes with this choice. Thus, for every n

$$\frac{1}{2\Delta t}(\|\mathbf{u}_h^{n+1}\|^2 - \|\mathbf{u}_h^n\|^2) + \nu\|\nabla \mathbf{u}_h^{n+1/2}\|^2 \leqslant \frac{1}{2\nu}\|\mathbf{f}^{n+1/2}\|_*^2 + \frac{\nu}{2}\|\nabla \mathbf{u}_h^{n+1/2}\|^2,$$

i.e.,

$$\frac{1}{\Delta t}(\|\mathbf{u}_h^{n+1}\|^2 - \|\mathbf{u}_h^n\|^2) + \nu\|\nabla \mathbf{u}_h^{n+1/2}\|^2 \leqslant \frac{1}{\nu}\|\mathbf{f}^{n+1/2}\|_*^2.$$

Summing from $n = 0 \ldots M - 1$ gives the bound (3.3).

Restricting to any particular time level n, the scheme is linear, and thus since it is also finite dimensional, uniqueness of solutions gives existence as well. Following the proof for the á priori bound, uniqueness is immediate at any time level. Thus solutions exist uniquely for the entire scheme.

$$\square$$

Remark 3.1. Since the kinetic energy $KE(\mathbf{u}_h^n) := \frac{1}{2}\|\mathbf{u}_h^n\|^2$ and energy dissipation $\varepsilon(\mathbf{u}_h^n) := \nu\|\nabla \mathbf{u}_h^n\|^2$ of NS-$\overline{\omega}$, take the usual form, it holds

$$KE(\mathbf{u}_M^h) + \nu \Delta t \sum_{n=0}^{M-1} \varepsilon(\mathbf{u}_{n+1/2}^h) = KE(\mathbf{u}_0^h) + \Delta t \sum_{n=0}^{M-1} (\mathbf{f}^{n+1/2}, \mathbf{u}_h^{n+1/2}). \qquad (3.4)$$

Thus, if $\nu = 0$ and $\mathbf{f} = \mathbf{0}$, $KE(\mathbf{u}_M^h) = KE(\mathbf{u}_0^h)$. Hence Algorithm 2.1 is energy conserving.

3.2. Convergence Analysis

Our main convergence result for the discrete NS-$\overline{\omega}$ model described in Algorithm 2.1 is given next.

Theorem 3.1 (Convergence for discrete NS-$\overline{\omega}$). *Consider the discrete NS-$\overline{\omega}$ model. Let $(\mathbf{w}(t), p(t))$ be a smooth, strong solution of the NSE such that the norms on the right hand side of (3.5)-(3.6) are finite. Suppose $(\mathbf{u}_h^0, p_h^0)$ are the $\mathbf{V}_h^{SV}$ and Q_h^{SV} interpolants of $(\mathbf{w}(0), p(0))$, respectively. Suppose $(\mathbf{u}_h, q_h)$ satisfies the scheme (2.21)-(2.22). Then there is a constant $C = C(\mathbf{w}, p)$ such that*

$$|||\mathbf{w} - \mathbf{u}_h|||_{\infty,0} \leqslant F(\triangle t, h, \alpha) + Ch^{k+1}|||\mathbf{w}|||_{\infty,k+1}, \quad (3.5)$$

$$\left(\nu\triangle t \sum_{n=0}^{M-1} \|\nabla(\mathbf{w}^{n+1/2} - (\mathbf{u}_h^{n+1} + \mathbf{u}_h^n)/2)\|^2\right)^{1/2} \leqslant F(\triangle t, h, \alpha) + C\nu^{1/2}(\triangle t)^2\|\nabla\mathbf{w}_{tt}\|_{2,0}$$

$$+ C\nu^{1/2}h^k|||\mathbf{w}|||_{2,k+1}, \quad (3.6)$$

where

$$\begin{aligned}
F(\triangle t, h, \alpha) &:= C^*\{(\nu + \nu^{-1})^{1/2}h^k|||\mathbf{w}|||_{2,k+1} \\
&+ \nu^{-1/2}h^k\left(|||\mathbf{w}|||_{4,k+1}^2 + |||\nabla\mathbf{w}_{1/2}|||_{4,0}^2\right) \\
&+ C(N)(\Delta t)^2\left(\|\mathbf{w}_{ttt}\|_{2,0} + \|\mathbf{f}_{tt}\|_{2,0} + (\nu + \nu^{-1})^{1/2}\|\nabla\mathbf{w}_{tt}\|_{2,0}\right) \\
&+ \nu^{-1/2}(\triangle t^2 + \alpha^{2N+2} + \alpha h^k + h^k)|||\nabla\mathbf{w}_{1/2}|||_{2,0}\}. \quad (3.7)
\end{aligned}$$

Remark 3.2. There are three important points to note from the theorem. First, the velocity error does not depend at all on the pressure error. Second, optimal accuracy can be achieved if $\alpha \leqslant O(h)$, and $2N + 2 \geqslant k$, which provides a guide for parameter selection. Finally, there is no time step restriction for the result; typically there is a strong restriction on the timestep resulting from using the Gronwall inequality, but our analysis allowed for a less restrictive discrete Gronwall inequality and no restriction on the time step.

Proof of Theorem 3.1. This proof closely follows the convergence estimate in [25], except for a few subtle differences that lead to improved estimates herein. Hence we give a shortened proof of the theorem, which highlights these differences.

Let

$$b_\omega(\mathbf{u}_h^{n+1/2}, \mathbf{v}_h^{n+1/2}, \boldsymbol{\chi}_h^{n+1/2}) := ((\nabla \times D_N^h F_h(\frac{3}{2}\mathbf{u}_h^n - \frac{1}{2}\mathbf{u}_h^{n-1})) \times \mathbf{v}_h^{n+1/2}, \boldsymbol{\chi}_h^{n+1/2}),$$

and, then by adding and subtracting terms, we can write

$$b_\omega(\mathbf{u}_h^{n+1/2}, \mathbf{v}_h^{n+1/2}, \boldsymbol{\chi}_h^{n+1/2}) = b(\mathbf{u}_h^{n+1/2}, \mathbf{v}_h^{n+1/2}, \boldsymbol{\chi}_h^{n+1/2}) - FE(\mathbf{u}_h^{n+1/2}, \mathbf{v}_h^{n+1/2}, \boldsymbol{\chi}_h^{n+1/2}),$$

where the linear extrapolated deconvolved filtering error FE is given by

$$FE(\mathbf{u}_h^{n+1/2}, \mathbf{v}_h^{n+1/2}, \boldsymbol{\chi}_h^{n+1/2}) := ((\nabla \times \mathbf{u}_h^{n+1/2} - \nabla \times D_N^h F_h(\frac{3}{2}\mathbf{u}_h^n - \frac{1}{2}\mathbf{u}_h^{n-1})) \times \mathbf{v}_h^{n+1/2}, \boldsymbol{\chi}_h^{n+1/2}).$$

At time $t_{n+1/2}$, the solution of the NSE $(\mathbf{w}, p)$ satisfies

$$\left(\frac{\mathbf{w}^{n+1} - \mathbf{w}^n}{\Delta t}, \mathbf{v}_h\right) + b_\omega(\mathbf{w}^{n+1/2}, \mathbf{w}^{n+1/2}, \mathbf{v}_h) + \nu(\nabla\mathbf{w}^{n+1/2}, \nabla\mathbf{v}_h)$$

$$= (\mathbf{f}^{n+1/2}, \mathbf{v}_h) + Intp(\mathbf{w}^n, \mathbf{v}_h), \quad \forall\mathbf{v}_h \in \mathbf{V}_h^{SV} \quad (3.8)$$

where the pressure term disappears since $\mathbf{V}_h^{SV}$ is now pointwise div-free, as stated in Section 2. The term $Intp(\mathbf{w}^n, \mathbf{v}_h)$ collects the interpolation error, the above linear extrapolated deconvolved filtering error, and the consistency error. It is given by

$$
\begin{aligned}
Intp(\mathbf{w}^n, \mathbf{v}_h) = {} & \left(\frac{\mathbf{w}^{n+1} - \mathbf{w}^n}{\Delta t} - \mathbf{w}_t(t_{n+1/2}), \mathbf{v}_h \right) + \nu(\nabla \mathbf{w}^{n+1/2} - \nabla \mathbf{w}(t_{n+1/2}), \nabla \mathbf{v}_h) \\
& + b_\omega(\mathbf{w}^{n+1/2}, \mathbf{w}^{n+1/2}, \mathbf{v}_h) - b_\omega(\mathbf{w}(t_{n+1/2}), \mathbf{w}(t_{n+1/2}), \mathbf{v}_h) \\
& - FE(\mathbf{w}(t_{n+1/2}), \mathbf{w}(t_{n+1/2}), \mathbf{v}_h) \\
& + \mathbf{f}(t_{n+1/2}) - \mathbf{f}_{n+1/2}, \mathbf{v}_h).
\end{aligned}
\tag{3.9}
$$

Subtracting (3.8) from (2.21) and letting $\mathbf{e}^n = \mathbf{w}^n - \mathbf{u}_h^n$ we have

$$
\begin{aligned}
\frac{1}{\Delta t}(\mathbf{e}^{n+1} - \mathbf{e}^n, \mathbf{v}_h) & + b_\omega(\mathbf{w}^{n+1/2}, \mathbf{w}^{n+1/2}, \mathbf{v}_h) - b_\omega(\mathbf{u}_h^{n+1/2}, \mathbf{u}_h^{n+1/2}, \mathbf{v}_h) \\
& + \nu(\nabla \mathbf{e}^{n+1/2}, \nabla \mathbf{v}_h) = Intp(\mathbf{w}^n, \mathbf{v}_h) \ , \quad \forall \mathbf{v}^h \in \mathbf{V}_h^{SV}.
\end{aligned}
\tag{3.10}
$$

where the pressure term of NS-$\overline{\omega}$ disappears since $\mathbf{V}_h^{SV}$ is now pointwise div-free. Decompose the error as $\mathbf{e}^n = (\mathbf{w}^n - \mathbf{U}^n) - (\mathbf{u}_h^n - \mathbf{U}^n) := \boldsymbol{\eta}^n - \boldsymbol{\phi}_h^n$ where $\boldsymbol{\phi}_h^n \in \mathbf{V}_h^{SV}$, and $\mathbf{U}$ is the L^2 projection of $\mathbf{w}$ in $\mathbf{V}_h^{SV}$. Setting $\mathbf{v}_h = \boldsymbol{\phi}_h^{n+1/2}$ in (3.10) we obtain

$$
\begin{aligned}
\frac{1}{2}(\|\boldsymbol{\phi}_h^{n+1}\|^2 - \|\boldsymbol{\phi}_h^n\|^2) + \nu\Delta t\|\nabla\boldsymbol{\phi}_h^{n+1/2}\|^2 = {} & (\boldsymbol{\eta}^{n+1} - \boldsymbol{\eta}^n, \boldsymbol{\phi}_h^{n+1/2}) + \triangle t\nu(\nabla\boldsymbol{\eta}^{n+1/2}, \nabla\boldsymbol{\phi}_h^{n+1/2}) \\
& + \triangle t\, b_\omega(\boldsymbol{\eta}^{n+1/2}, \mathbf{w}^{n+1/2}, \boldsymbol{\phi}_h^{n+1/2}) - \triangle t\, b_\omega(\boldsymbol{\phi}_h^{n+1/2}, \mathbf{w}^{n+1/2}, \boldsymbol{\phi}_h^{n+1/2}) \\
& + \triangle t\, b_\omega(\mathbf{u}_h^{n+1/2}, \boldsymbol{\eta}^{n+1/2}, \boldsymbol{\phi}_h^{n+1/2}) + \triangle t\, Intp(\mathbf{w}^n, \boldsymbol{\phi}_h^{n+1/2}) \\
= {} & T_1 + T_2 + T_3 + T_4 + T_5 + T_6\,.
\end{aligned}
\tag{3.11}
$$

We point out again that, this error equation we will proceed to analyze, is independent of pressure error, which occurs due to the use of Scott-Vogelius elements and would not happen if, for example, Taylor-Hood elements were chosen.

Estimates for the right hand side terms of (3.11) follow similar to those in the convergence proof in [25], except for the last three terms. For the last term, the main difference is the use of deconvolution, and so one can follow estimates in [31, 24] to bound this term. Thus we proceed to estimate T_4 and T_5 terms of (3.11). For T_4 term, using (2.6), we get

$$
\begin{aligned}
\triangle t\, b_\omega(\boldsymbol{\phi}_h^{n+1/2}, \mathbf{w}^{n+1/2}, \boldsymbol{\phi}_h^{n+1/2}) & = \triangle t\, (\nabla \times D_N^h F_h(\tfrac{3}{2}\boldsymbol{\phi}_h^n - \tfrac{1}{2}\boldsymbol{\phi}_h^{n-1}) \times \mathbf{w}^{n+1/2}, \boldsymbol{\phi}_h^{n+1/2}) \\
& \leqslant C\triangle t \left\|\mathbf{w}^{n+1/2}\right\|_2 \left\|\nabla\boldsymbol{\phi}_h^{n+1/2}\right\| \left\|D_N^h F_h(\tfrac{3}{2}\boldsymbol{\phi}_h^n - \tfrac{1}{2}\boldsymbol{\phi}_h^{n-1})\right\| \\
& \leqslant C(N)\triangle t \left\|\mathbf{w}^{n+1/2}\right\|_2 \left\|\nabla\boldsymbol{\phi}_h^{n+1/2}\right\| (\|\boldsymbol{\phi}_h^n\| + \|\boldsymbol{\phi}_h^{n-1}\|) \\
& \leqslant \frac{\nu\triangle t}{12}\|\nabla\boldsymbol{\phi}_h^{n+1/2}\|^2 + C(N)\triangle t\,\nu^{-1}(\|\boldsymbol{\phi}_h^n\|^2 + \|\boldsymbol{\phi}_h^{n-1}\|^2)\|\mathbf{w}^{n+1/2}\|_2^2\,.
\end{aligned}
$$

For T_5 term, we begin by splitting the first entry of this term by adding and subtracting $\mathbf{w}_{n+1/2}$, followed by rewriting the resulting error term as pieces inside and outside of the finite element space.

$$
\begin{aligned}
\triangle t b_\omega(\mathbf{u}_h^{n+1/2}, \boldsymbol{\eta}^{n+1/2}, \boldsymbol{\phi}_h^{n+1/2}) = {} & \triangle t b_\omega(\boldsymbol{\eta}^{n+1/2}, \boldsymbol{\eta}^{n+1/2}, \boldsymbol{\phi}_h^{n+1/2}) \\
& + \triangle t b_\omega(\boldsymbol{\phi}_h^{n+1/2}, \boldsymbol{\eta}^{n+1/2}, \boldsymbol{\phi}_h^{n+1/2}) + \triangle t b_\omega(\mathbf{w}^{n+1/2}, \boldsymbol{\eta}^{n+1/2}, \boldsymbol{\phi}_h^{n+1/2}).
\end{aligned}
\tag{3.12}
$$

For the first and last terms of the above equation (3.12), usual estimates give

$$\triangle t b_{\omega}(\boldsymbol{\eta}^{n+1/2}, \boldsymbol{\eta}^{n+1/2}, \boldsymbol{\phi}_h^{n+1/2})$$
$$\leqslant \frac{\nu \triangle t}{24}\|\nabla\boldsymbol{\phi}_h^{n+1/2}\|^2 + C(N)\triangle t\nu^{-1}(\|\nabla\boldsymbol{\eta}^n\|^2 + \|\nabla\boldsymbol{\eta}^{n-1}\|^2)\|\nabla\boldsymbol{\eta}^{n+1/2}\|^2 ,$$

$$\triangle t b_{\omega}(\mathbf{w}^{n+1/2}, \boldsymbol{\eta}^{n+1/2}, \boldsymbol{\phi}_h^{n+1/2}) \leqslant \frac{\nu\triangle t}{24}\|\nabla\boldsymbol{\phi}_h^{n+1/2}\|^2 + C(N)\triangle t\nu^{-1}\|\nabla\boldsymbol{\eta}^{n+1/2}\|^2 .$$

The second term of (3.12) is a bit more delicate, and is majorized as

$$\triangle t b_{\omega}(\boldsymbol{\phi}_h^{n+1/2}, \boldsymbol{\eta}^{n+1/2}, \boldsymbol{\phi}_h^{n+1/2}) = \triangle t(\nabla \times D_N^h F_h(\frac{3}{2}\boldsymbol{\phi}_h^n - \frac{1}{2}\boldsymbol{\phi}_h^{n-1}) \times \boldsymbol{\eta}^{n+1/2}, \boldsymbol{\phi}_h^{n+1/2})$$

$$\leqslant \triangle t|(\boldsymbol{\phi}_h^{n+1/2} \times \boldsymbol{\eta}^{n+1/2}, \nabla \times D_N^h F_h(\frac{3}{2}\boldsymbol{\phi}_h^n - \frac{1}{2}\boldsymbol{\phi}_h^{n-1}))|$$

$$\leqslant \triangle t|(\boldsymbol{\phi}_h^{n+1/2} \cdot \nabla\boldsymbol{\eta}^{n+1/2}, D_N^h F_h(\frac{3}{2}\boldsymbol{\phi}_h^n - \frac{1}{2}\boldsymbol{\phi}_h^{n-1}))|$$

$$\qquad + \triangle t|(\boldsymbol{\eta}_h^{n+1/2} \cdot \nabla\boldsymbol{\phi}^{n+1/2}, D_N^h F_h(\frac{3}{2}\boldsymbol{\phi}_h^n - \frac{1}{2}\boldsymbol{\phi}_h^{n-1}))|$$

$$\leqslant C(N)\triangle t \left\|\nabla\boldsymbol{\eta}_h^{n+1/2}\right\| \left\|\nabla\boldsymbol{\phi}^{n+1/2}\right\| \left\|\frac{3}{2}\boldsymbol{\phi}_h^n - \frac{1}{2}\boldsymbol{\phi}_h^{n-1}\right\|^{1/2} \left\|\nabla(\frac{3}{2}\boldsymbol{\phi}_h^n - \frac{1}{2}\boldsymbol{\phi}_h^{n-1})\right\|^{1/2}$$

$$\leqslant C(N)h^{-1/2}\triangle t \left\|\nabla\boldsymbol{\eta}_h^{n+1/2}\right\| \left\|\nabla\boldsymbol{\phi}^{n+1/2}\right\| \left\|\frac{3}{2}\boldsymbol{\phi}_h^n - \frac{1}{2}\boldsymbol{\phi}_h^{n-1}\right\|$$

$$\leqslant \frac{\nu\triangle t}{12}\|\nabla\boldsymbol{\phi}_h^{n+1/2}\|^2 + C(N)\triangle t\,\nu^{-1}h^{-1}\,(\|\boldsymbol{\phi}_h^n\|^2 + \|\boldsymbol{\phi}_h^{n-1}\|^2)\|\nabla\boldsymbol{\eta}^{n+1/2}\|^2.$$

Combining estimates and summing from $n = 1$ to M (assuming that $\|\boldsymbol{\phi}_h^0\| = 0$) reduces (3.11) to

$$\|\boldsymbol{\phi}_h^M\|^2 + \nu\triangle t \sum_{n=1}^{M-1}\|\nabla\boldsymbol{\phi}_h^{n+1/2}\|^2$$

$$\leqslant C\triangle t\{\sum_{n=1}^{M-1} C\nu^{-1}\,(\|\mathbf{w}^{n+1/2}\|_2^2 + h^{-1}\|\nabla\boldsymbol{\eta}^{n+1/2}\|^2)(\|\boldsymbol{\phi}_h^n\|^2 + \|\boldsymbol{\phi}_h^{n-1}\|^2)$$

$$+ \sum_{n=1}^{M-1}\left((\nu + \nu^{-1})\|\nabla\boldsymbol{\eta}^{n+1/2}\|^2 + \nu^{-1}\,(\|\nabla\boldsymbol{\eta}^n\|^2 + \|\nabla\boldsymbol{\eta}^{n-1}\|^2)\|\nabla\mathbf{w}^{n+1/2}\|^2\right.$$

$$+ \nu^{-1}(\|\nabla\boldsymbol{\eta}^n\|^2 + \|\nabla\boldsymbol{\eta}^{n-1}\|^2)\|\nabla\boldsymbol{\eta}^{n+1/2}\|^2) + \sum_{n=1}^{M-1} |Intp(\mathbf{w}_n, \boldsymbol{\phi}_{n+1/2}^h)|\,\}$$

$$\leqslant C\triangle t\{\sum_{n=1}^{M-1} C\nu^{-1}\,(\|\mathbf{w}^{n+1/2}\|_2^2 + h^{-2}\|\nabla\boldsymbol{\eta}^{n+1/2}\|^2)\|\boldsymbol{\phi}_h^n\|^2$$

$$+ (\nu + \nu^{-1}) \sum_{n=1}^{M-1}\|\nabla\boldsymbol{\eta}^{n+1/2}\|^2 + \nu^{-1} \sum_{n=0}^{M-1}\|\nabla\boldsymbol{\eta}^n\|^2\|\nabla\mathbf{w}^{n+1/2}\|^2$$

$$+ \nu^{-1} \sum_{n=0}^{M}\|\nabla\boldsymbol{\eta}^n\|^4 + \sum_{n=1}^{M-1} |Intp(\mathbf{w}_n, \boldsymbol{\phi}_{n+1/2}^h)|\,\}. \tag{3.13}$$

From here, standard techniques will finish the proof, except for one subtle difference: the alternate Gronwall lemma (e.g., of [16]) can be used since no $\|\phi^M\|^2$ appears on the right hand side. This implies no timestep restriction is needed, and the constants that arise will depend on ν^{-1} instead of ν^{-3} [20].

3.3. An alternative choice of α

It is common in 'α-models' for the choice of filtering radius parameter to be chosen on the order of the meshwidth, $\alpha = O(h)$. From the preceding error analysis, it can be seen that such a choice of α is the largest it can be without creating suboptimal asymptotic accuracy. Although this provides some guidance on the choice of α, finding an optimal α on a particular fixed mesh still may require some tuning. We describe now a connection between NS-$\overline{\omega}$ and the velocity-vorticity-helicity (VVH) formulation of the NSE [34], that suggests an alternative choice of α that may aid in this process.

NS-$\overline{\omega}$ can be considered as a rotational form of the NSE formulation where the vorticity term is handled by other equations, which for NS-$\overline{\omega}$ is the regularization equations. Such a formulation is quite similar to a velocity-vorticity method, where the vorticity comes directly from solving the vorticity equation. In particular, consider the numerical method devised in [34] for the VVH NSE formulation

Algorithm 3.1.
Step 1. Given $\mathbf{u}^n$, $\mathbf{u}^{n-1}$, $\mathbf{w}^n$ and $\mathbf{u}^* = \frac{3}{2}\mathbf{u}^n - \frac{1}{2}\mathbf{u}^{n-1}$, find $\mathbf{w}^{n+1}$ and $hel^{n+1/2}$ from

$$\frac{\mathbf{w}^{n+1} - \mathbf{w}^n}{\triangle t} - \nu\triangle\mathbf{w}^{n+1/2} + 2D(\mathbf{w}^{n+1/2})\mathbf{u}^* - \nabla hel^{n+1/2} = \nabla \times \mathbf{f}^{n+1/2} \qquad (3.14)$$

$$\nabla \cdot \mathbf{w}^{n+1} = 0 \qquad (3.15)$$

$$\mathbf{w}^{n+1} = \nabla \times (2\mathbf{u}^n - \mathbf{u}^{n-1}) \text{ on } \partial\Omega \qquad (3.16)$$

Step 2. Given $\mathbf{u}^n$, $\mathbf{w}^n$ and $\mathbf{w}^{n+1}$, find $\mathbf{u}^{n+1}$ and $P^{n+1/2}$

$$\frac{\mathbf{u}^{n+1} - \mathbf{u}^n}{\triangle t} - \nu\triangle\mathbf{u}^{n+1/2} + \mathbf{w}^{n+1/2} \times \mathbf{u}^{n+1/2} - \nabla P^{n+1/2} = \mathbf{f}^{n+1/2} \qquad (3.17)$$

$$\nabla \cdot \mathbf{u}^{n+1} = 0 \qquad (3.18)$$

$$\mathbf{u}^{n+1} = \boldsymbol{\phi} \text{ on } \partial\Omega \qquad (3.19)$$

where $\boldsymbol{\phi}$ is the Dirichlet boundary condition function and $D(\cdot)$ denotes the deformation tensor, i.e., $D(\mathbf{v}) = \frac{(\nabla\mathbf{v})+(\nabla\mathbf{v})^T}{2}$, $\mathbf{u}, \mathbf{w}$ denote velocity and vorticity, P is the Bernoulli pressure and hel is helical density.

If $\mathbf{f}$ is irrotational and we remove the nonlinear term from the vorticity equation, this system is analogous to the NS-$\overline{\omega}$ scheme herein if we identify helical density with the Lagrange multiplier λ corresponding to the incompressibility of the filtered velocity, and $\nu\Delta t$ with α^2, i.e., $\alpha = \sqrt{\nu\Delta t}$. Choosing an optimal filtering radius α is certainly problem dependent, and by no means are we suggesting this choice is always optimal. However, our numerical experiments show it can be a good starting point for choosing α when using NS-$\overline{\omega}$.

$\square$

4. Numerical experiments

In this section, we present several numerical experiments that demonstrate the effectiveness of the numerical method studied herein. The first two experiments are for benchmark tests of channel flow over a step and around a cylinder, respectively, and both show excellent results when α is chosen as we suggest herein. The third and fourth tests are done with Scott-Vogelius elements and Taylor-Hood elements, and compare solutions for a problem with known analytical solution and the cylinder problem. All tests are done using our Matlab code, and linear solver uses the 'slash' command. Of course, such a solver is non-optimal for saddle point problems, and for larger 3D problems, a more sophisticated linear solver will be needed to solve the saddle point system. This will be addressed in future work.

4.1. Experiment 1: Channel flow over a forward-backward facing step

Our first numerical experiment is for the benchmark 2D problem of channel flow over a forward-backward facing step. The domain Ω is a 40x10 rectangle with a 1x1 step 5 units into the channel at the bottom. The top and bottom of the channel as well as the step are prescribed with no-slip boundary conditions, and the sides are given the parabolic profile $(y(10-y)/25, 0)^T$. We use the initial condition of $\mathbf{u}_0 = (y(10-y)/25, 0)^T$ inside Ω, and run the test to $T = 40$. For a chosen viscosity $\nu = 1/600$, it is known that the correct behavior is for an eddy to form behind the step, grow, detach from the step to move down the channel, and a new eddy forms. For a more detailed description of the problem, see [15, 19]. The eddy formation and separation present in this test problem is part of a complex flow structure, and its capture is critical for an effective fluid flow model. Moreover, a useful fluid model will correctly predict this behavior on a coarser mesh than can a direct numerical simulation of the NSE.

For the following test, we computed Algorithm 2.1 with (P_2, P_1^{disc}) Scott-Vogelius elements on a barycenter-refinement of a Delauney triangulated mesh, yielding 14,467 total degrees of freedom, with deconvolution order $N = 1$, and varying α. This mesh provided a smallest element width of 0.15 units behind the step, and largest of 1.9 units, at the top of the channel around $x = 30$. For comparison, we also directly compute the (non-regularized) NSE ($\alpha = N = 0$). We compute first with timestep $\Delta t = 0.05$, and the solutions at $T = 40$ are shown in Fig. 4.1. Several interesting observations can be made; first, we note that the optimal choice of α appears to be near $\alpha = \sqrt{\nu \Delta t}$, as this is the only solution to predict a smooth flow field and eddies forming and detaching behind the step. For the NSE ($\alpha = 0$), a smooth flow field is predicted, however the eddies behind the step appear to be stretching instead of detaching. Larger values of α, including the common choice of the average element width $\alpha = h = 0.627$, give increasingly worse solutions. This is somewhat counterintuitive, as α is a filtering radius that is supposed to regularize and thus smooth oscillations. A closer examination reveals that the oscillations are arising from an inability of the more regularized models to resolve the flow at the top left corner of the step, where the flow near the bottom of the channel is forced up to intersect with the free stream.

To test the scaling of optimal α with Δt, we compute with the same data, but with timesteps $\Delta t = 0.01$ and 0.025, with parameter $\alpha = \sqrt{\nu \Delta t}$. The results at $T = 40$ are shown in Figure 4.2, and show good results in both cases. However, for the smaller timestep, we see the eddies stretching instead of detaching. This is not surprising, as one should expect some h-dependence on the choice of α.
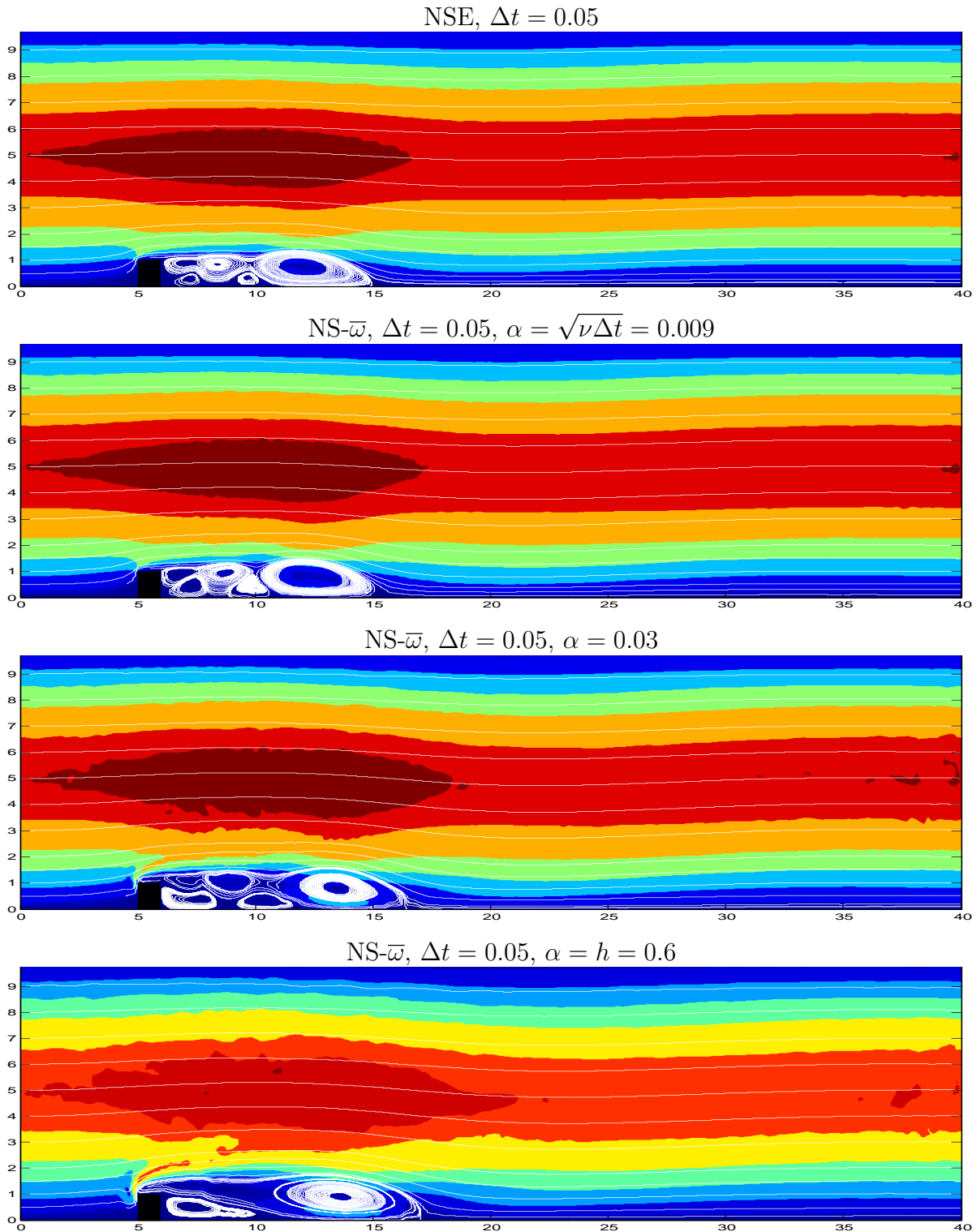
Figure 4.1. Shown above are the $T = 40$ SV solutions as velocity streamlines over speed contours for the step problem from Experiment 1. Shown are the NSE (top) which is somewhat underresolved on this mesh as the eddies are not fully detaching, NS-$\overline{\omega}$ with $\alpha = \sqrt{\nu \Delta t}$ (second from top) which agrees with the known true solution, NS-$\overline{\omega}$ with $\alpha = 0.3$ (third from top) which has oscillations present in the speed contours, and NS-$\overline{\omega}$ with $\alpha = h = 0.6$ (bottom) which is a poor approximation. All of the solutions are pointwise divergence-free
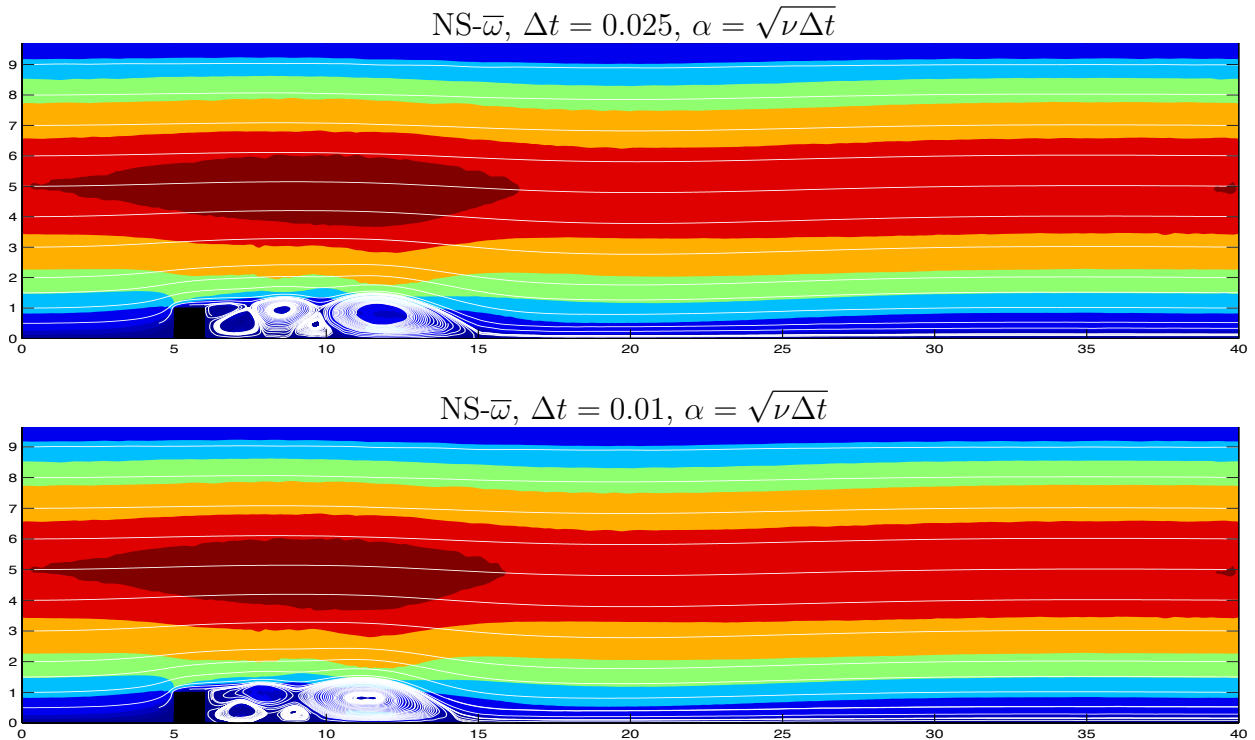
Figure 4.2. Shown above are the $T = 40$ SV solutions as velocity streamlines over speed contours for the step problem from Experiment 1, with parameter chosen as $\alpha = \sqrt{\nu \Delta t}$, for varying timesteps

4.2. Experiment 2: Channel flow around a cylinder

The benchmark problem of 2d channel flow around a cylinder has been studied in numerous works, e.g., [18, 20, 23, 37], and is well documented in [37]. The domain is the rectangle $[0, 2.2] \times [0, 0.41]$ representing the channel with flow in the positive x direction, with a circle radius 0.05 centered at $(0.2, 0.2)$ representing the cylinder. No slip boundary conditions are prescribed on the top and bottom of the channel as well as on the cylinder, and the time dependent inflow and outflow velocity profiles are given by

$$\mathbf{u}(0, y, t) = \mathbf{u}(2.2, y, t) = \left[\frac{6}{0.41^2} \sin(\pi t/8) y (0.41 - y), 0 \right]^T, \quad 0 \leqslant y \leqslant 0.41.$$

The forcing function is set to zero, $\mathbf{f} = \mathbf{0}$, and the viscosity at $\nu = 0.001$, providing a time dependent Reynolds number, $0 \leqslant Re(t) \leqslant 100$. The initial condition is $\mathbf{u} = \mathbf{0}$, and we compute to final time $T = 8$ with timestep $\Delta t = 0.005$. An accurate approximation of this flow's velocity field will show a vortex street forming behind the cylinder by $t = 4$, and a fully formed vortex street by $t = 7$.

We test the algorithm with $\alpha = h = 0.01084$ and $\alpha = \sqrt{\nu \Delta t}$, on a barycenter refined mesh that provides 26,656 degrees of freedom for (P_2, P_1^{disc}) Scott-Vogelius elements (minimum and maximum element widths were 0.0042 and 0.017 respectively), and again find that $\alpha = \sqrt{\nu \Delta t}$ provides a better solution than $\alpha = h$. These results are shown for $t = 7$ in Fig. 4.3. The $\alpha = \sqrt{\nu \Delta t}$ solution agrees with documented DNS results [7, 23], but the $\alpha = h$ solution at $t = 7$ is observed to be incorrect, as it does not fully resolve the wake, and its speed contours show it gives a much different (and thus incorrect) solution behind the cylinder.

SV elements, $\alpha = h = 0.01$

SV elements, $\alpha = \sqrt{\nu \Delta t} = 0.0022$
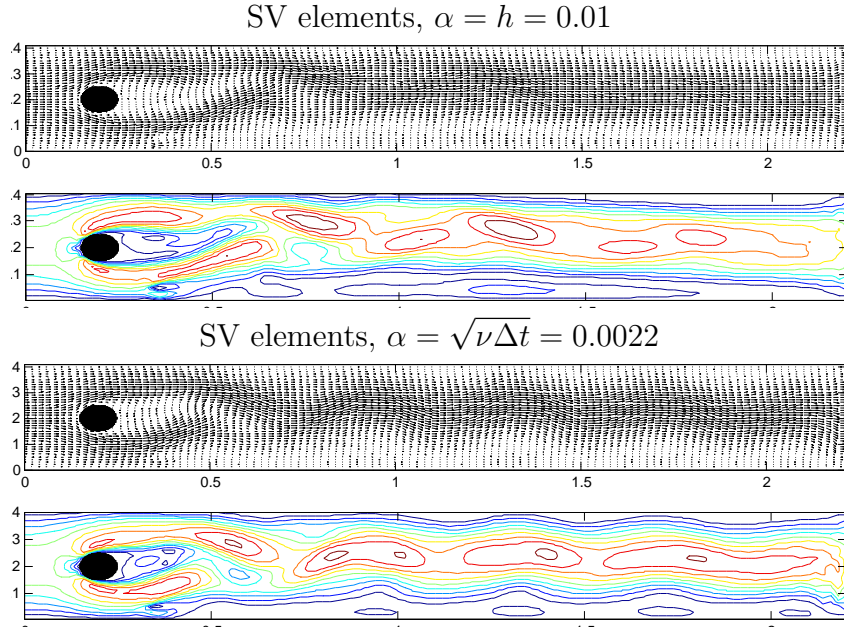
Figure 4.3. The above pictures show the velocity fields and speed contours at $t = 7$ using Scott-Vogelius elements with $\alpha = h$ (top) and $\alpha = \sqrt{\nu \Delta t}$ (bottom). The $\alpha = h$ solution is under-resolved, as it loses resolution of the vortex street, and its speed contours are inaccurate. The $\alpha = \sqrt{\nu \Delta t}$ solution captures the entire wake, and its speed contours agree well with the known solution

*4.2.1. **Comparison to Taylor-Hood element solution*** Using the same problem data as Experiment 2 above, we also compute using (P_2, P_1) Taylor-Hood elements, with $\alpha = \sqrt{\nu \Delta t}$ (which gave about the same answer as for $\alpha = h$). Since this element pair is widely used and is closely related to Scott-Vogelius elements (they differ only in the pressure space being continuous or not), a comparison is of interest. Since Taylor-Hood uses a continuous pressure space, with the same mesh the total number of degrees of freedom is 17,306. All of problem data is kept the same, and results are shown in Figs. 4.4 and 4.5. In Fig. 4.4, we observe that the Taylor-Hood solution is much worse than the Scott-Vogelius solution shown in Fig. 4.3; the Taylor-Hood solution fails to resolve the important behavior behind the cylinder. Figure 4.5 shows mass conservation versus time for the Taylor-Hood and Scott-Vogelius solutions. As expected, the Scott-Vogelius solution is divergence-free up to machine precision. The mass conservation offered by the Taylor-Hood solution is poor. Even though, asymptotically, the divergence error is optimal, on coarse meshes (where one would hope to use regularization models) the actual error can be bad. However, on average the linear solver took 0.700 seconds for the SV element while the linear solver for the TH element only required 0.490 seconds.

It is not surprising that the Taylor-Hood solution is much worse than the Scott-Vogelius solution. It was shown in [23] that for the rotational form NSE, the Bernoulli pressure error can be large enough to dramatically reduce velocity error for this problem. Since NS-$\overline{\omega}$ is also rotational form, this same effect can be expected (and is seen in comparing Fig. 4.3 to Fig. 4.4). However, for the Scott-Vogelius solution, as shown herein, the velocity error is independent of the pressure error. Thus even though the pressure error may be large, it has no adverse effect on the velocity error, leaving the good solution seen in Fig. 4.3.
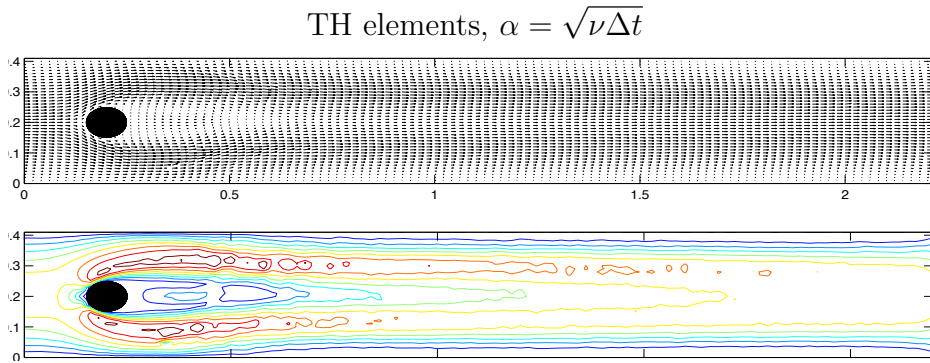
TH elements, $\alpha = \sqrt{\nu \Delta t}$

Figure 4.4. The above picture shows the $t = 7$ solution using Taylor-Hood elements, as velocity vector field and speed contours. This solution is incorrect, as it fails to capture any wake behind the cylinder
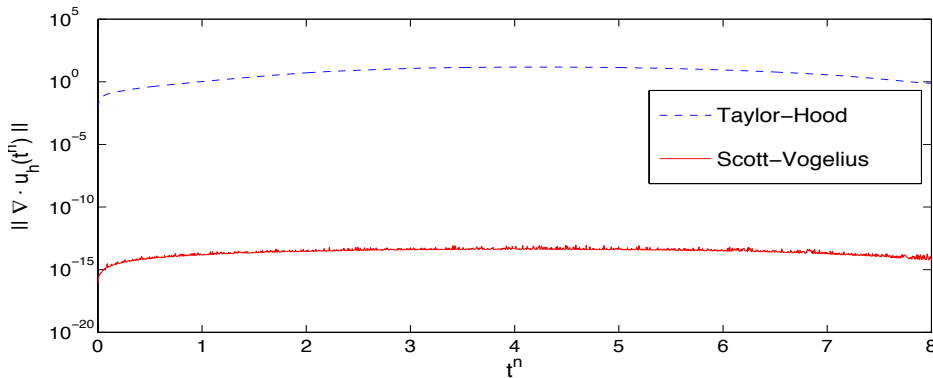
Figure 4.5. Shown above are the plots of the L^2 norms of the divergence of the velocity solutions versus time, for the SV and TH solutions, both with $\alpha = \sqrt{\nu \Delta t} = 0.0022$

As expected, the Scott-Vogelius solution is incompressible to near machine precision. The Taylor-Hood solution, however, gives poor mass conservation.

4.3. Experiment 3: Effect of pressure error on velocity error

In this experiment, we investigate more closely the effect of the pressure error on the velocity error, which caused a dramatic difference between Scott-Vogelius and Taylor-Hood solutions in the above experiment of flow around a cylinder. The error analysis in Section 3.2 showed that in Algorithm 2.1 which uses Scott-Vogelius elements, the velocity error is not affected by the pressure error. If Taylor-Hood elements are used, however, then the energy error of the velocity can be shown to depend on $C(\nu^{-1})\Delta t \sum_{n=0}^{M-1} \inf_{r_h \in Q_h^{TH}} \|q - r_h\|$, e.g. [25], although the scaling by $C(\nu^{-1})$ of this term can be reduced by using grad-div stabilization [23, 31, 35].

To better demonstrate this effect, we compute Algorithm 2.1 with both Scott-Vogelius and Taylor-Hood elements, for a series of simple test problems with increasing pressure complexity and the same velocity solution. On the domain, $\Omega = (0,1)^2$ and $0 \leqslant t \leqslant 0.1 = T$, we choose

$$\mathbf{u} = (1 + 0.01t) \begin{pmatrix} \cos(y) \\ \sin(x) \end{pmatrix}, \quad p = x + y + \sin(n(x + y)),$$

which will solve the NSE with an appropriate function f.

Solutions are approximated to this solution on a quasi-uniform barycenter-refined mesh that provides 12,604 degrees of freedom with (P_2, P_1^{disc}) Scott-Vogelius elements (7,258 for velocity and 5,364 for pressure) and 8,182 degrees of freedom with (P_2, P_1) Taylor-Hood (7,258 for velocity and 924 for pressure), kinematic viscosity is set to be $\nu = 0.01$, timestep $\Delta t = 0.025$, $\alpha = \sqrt{\nu \Delta t} = 0.0158$, $N = 1$, mesh width $(h) = 0.0625$, and the parameter for pressure complexity $n = 0, 1, 2, 3$. The results are shown in Table 4.1, and as expected the error in the Scott-Vogelius velocity solution is unaffected by the increase in pressure complexity. However, the Taylor-Hood velocity solution significanty lost accuracy. Also included in the table is the size of the velocity divergence, measured in $L^2(0, T; L^2(\Omega))$. As expected, for the SV solution, near machine epsilon is found for each n, but for TH, the quantity is non-negligible and gets worse with increasing pressure complexity.

n	$\left\|\mathbf{u}_{NSE} - \mathbf{u}_h^{SV}\right\|_{2,1}$	$\left\|\nabla \cdot \mathbf{u}_h^{SV}\right\|_{2,0}$	$\left\|\mathbf{u}_{NSE} - \mathbf{u}_h^{TH}\right\|_{2,1}$	$\left\|\nabla \cdot \mathbf{u}_h^{TH}\right\|_{2,0}$
0	7.332E-5	1.106E-14	3.075E-3	2.775E-3
1	7.332E-5	1.167E-14	5.315E-3	4.763E-3
2	7.332E-5	1.102E-14	1.716E-2	1.533E-2
3	7.330E-5	8.724E-15	3.584E-2	3.235E-2

Table 4.1. Errors in velocity and divergence for Experiment 1 for Scott-Vogelius and Taylor-Hood elements used with Algorithm 2.1

References

[1] G. Baker, *Galerkin Approximations for the Navier-Stokes Equations*, Harvard University, 1976.

[2] M. Benzi and M. Olshanskii, *An augmented Lagrangian-based approach to the Oseen problem*, SIAM J. Sci. Comput., **28** (2006), pp. 2095–2113.

[3] L. Berselli, T. Iliescu, and W. J. Layton, *Mathematics of Large Eddy Simulation of Turbulent Flows*, Scientific Computation, Springer, 2006.

[4] A. Bowers and L. Rebholz, *Increasing accuracy and efficiency in FE computations of the Leray-deconvolution model*, Numerical Methods for Partial Differential Equations, (2010) DOI: 10.1002/num.20653.

[5] S. Brenner and L. Scott, *The Mathematical Theory of Finite Element Methods*, Springer-Verlag, 1994.

[6] E. Burman and A. Linke, *Stabilized finite element schemes for incompressible flow using Scott-Vogelius elements*, Applied Numerical Mathematics, **58** (2008), no. 11, pp. 1704–1719.

[7] M. Case, V. Ervin, A. Linke, and L. Rebholz, *Improving mass conservation in FE approximations of the NSE with C^0 velocities: A connection between Scott-Vogelius elements and grad-div stabilization*, Submitted, available as technical report as WIAS preprint 1510 at http://www.wias-berlin.de/preprint/1510/wias_preprints_1510.pdf, (2010).

[8] S. Chen, C. Foias, D. Holm, E. Olson, E. Titi, and S. Wynne, *The Camassa-Holm equations as a closure model for turbulent channel and pipe flow*, Phys. Rev. Lett., **81** (1998), pp. 5338–5341.

[9] S. Chen, D. Holm, L. Margolin, and R. Zhang, *Direct numerical simulations of the Navier-Stokes alpha model*, Physica D, **133** (1999), pp. 66–83.

[10] A. Cheskidov, D. Holm, E. Olson, and E. Titi, *On a Leray-alpha model of turbulence*, Royal Society London, Proceedings, Series A, Mathematical, Physical and Engineering Sciences, (2005), pp. 629–649.

[11] A. Dunca and Y. Epshteyn, *On the Stolz-Adams deconvolution model for the Large-Eddy simulation of turbulent flows*, SIAM J. Math. Anal., **37** (2005), no. 6, pp. 1890–1902.

[12] V. Ervin, W. Layton, and M. Neda, *Numerical analysis of filter based stabilization for evolution equations*, Submitted, available as technical report TR-MATH 10-01 from http://www.mathematics.pitt.edu/research/technical-reports.php, (2010).

[13] G. Galdi and W. Layton, *Approximating the larger eddies in fluid motion II: A model for space filtered flow*, Math. Methods and Models in Appl. Sci., **10** (2000), no. 3, pp. 1–8.

[14] M. Germano, *Differential filters for the large eddy numerical simulation of turbulent flows*, Physics of Fluids, **29** (1986), pp. 1755–1757.

[15] M. Gunzburger, *Finite Element Methods for Viscous Incompressible Flow: A Guide to Theory, Practice, and Algorithms*, Academic Press, Boston, 1989.

[16] J. Heywood and R. Rannacher, *Finite element approximation of the nonstationary Navier-Stokes problem. Part IV: Error analysis for the second order time discretization*, SIAM J. Numer. Anal., **2** (1990), pp. 353–384.

[17] D. Holm and B. Guerts, *Leray and LANS-α modelling of turbulent mixing*, J. of Turbulence, **7** (2006), no. 10.

[18] V. John, *Reference values for drag and lift of a two dimensional time-dependent flow around a cylinder*, International Journal for Numerical Methods in Fluids, **44** (2004), pp. 777–788.

[19] V. John and W. J. Layton, *Analysis of numerical errors in Large Eddy Simulation*, SIAM J. Numer. Anal., **40** (2002), no. 3, pp. 995–1020.

[20] A. Labovsky, W. Layton, C. Manica, M. Neda, and L. Rebholz, *The stabilized extrapolated trapezoidal finite element method for the Navier-Stokes equations*, Comput. Methods Appl. Mech. Engrg., **198** (2009), pp. 958–974.

[21] W. Layton, *A remark on regularity of an elliptic-elliptic singular perturbation problem*, Tech. rep., University of Pittsburgh, 2007.

[22] W. Layton, *The existence of smooth attractors for the NS-$\overline{\omega}$ model of turbulence*, Journal of Mathematical Analysis and Applications, **366** (2010), pp. 81–89.

[23] W. Layton, C. Manica, M. Neda, M. Olshanskii, and L. Rebholz, *On the accuracy of the rotation form in simulations of the Navier-Stokes equations*, J. Comput. Phys., **228** (2009), no. 5, pp. 3433–3447.

[24] W. Layton, C. Manica, M. Neda, and L. Rebholz, *Numerical analysis and computational testing of a high-accuracy Leray-deconvolution model of turbulence*, Numerical Methods for Partial Differential Equations, **24** (2008), no. 2, pp. 555–582.

[25] W. Layton, C. Manica, M. Neda, and L. Rebholz, *Numerical analysis and computational comparisons of the NS-omega and NS-alpha regularizations*, Comput. Methods Appl. Mech. Engrg., **199** (2010), pp. 916–931.

[26] W. Layton, I. Stanculescu, and C. Trenchea, *Theory of the NS-$\overline{\omega}$ model: A complement to the NS-alpha model*, Submitted, available as technical report TR-MATH08-18 at http://www.mathematics.pitt.edu/research/technical-reports.php, (2008).

[27] A. Linke, *Collision in a cross-shaped domain — A steady 2d Navier-Stokes example demonstrating the importance of mass conservation in CFD*, Comp. Meth. Appl. Mech. Eng., **198** (2009), no. 41–44, pp. 3278–3286.

[28] A. Linke, G. Matthies, and L. Tobiska, *Non-nested multi-grid solvers for mixed divergence free scott-vogelius discretizations*, Computing, **83** (2008), no. 2-3, pp. 87–107.

[29] E. Lunasin, S. Kurien, M. Taylor, and E. Titi, *A study of the Navier-Stokes-alpha model for two-dimensional turbulence*, Journal of Turbulence, **8** (2007), pp. 751–778.

[30] C. Manica and S. K. Merdan, *Convergence Analysis of the Finite Element Method for a fundamental model in turbulence*, Tech. rep., University of Pittsburgh, 2006.

[31] C. Manica, M. Neda, M. Olshanskii, and L. Rebholz, *Enabling accuracy of Navier-Stokes-alpha through deconvolution and enhanced stability*, M2AN: Mathematical Modelling and Numerical Analysis, **8** (2011), pp. 277–308.

[32] M. Olshanskii, *A low order Galerkin finite element method for the Navier-Stokes equations of steady incompressible flow: A stabilization issue and iterative methods*, Comp. Meth. Appl. Mech. Eng., **191** (2002), pp. 5515–5536.

[33] M. Olshanskii, G. Lube, T. Heister, and J. Löwe, *Grad-div stabilization and subgrid pressure models for the incompressible Navier-Stokes equations*, Comp. Meth. Appl. Mech. Eng., **198** (2009), pp. 3975–3988.

[34] M. Olshanskii and L. Rebholz, *Velocity-vorticity-helicity formulation and a solver for the Navier-Stokes equations*, Journal of Computational Physics, **229** (2010), pp. 4291–4303.

[35] M. Olshanskii and A. Reusken, *Grad-Div stabilization for the Stokes equations*, Math. Comp., **73** (2004), pp. 1699–1718.

[36] L. Rebholz and M. Sussman, *On the high accuracy NS-α-deconvolution model of turbulence*, Mathematical Models and Methods in Applied Sciences, **20** (2010), pp. 611–633.

[37] M. Schäfer and S. Turek, *The benchmark problem 'flow around a cylinder' flow simulation with high performance computers II*, in E.H. Hirschel (Ed.), Notes on Numerical Fluid Mechanics, **52**, Braunschweig, Vieweg (1996), pp. 547–566.

[38] M. Vogelius, *An analysis of the p-version of the finite element method for nearly incompressible materials. Uniformly valid, optimal error estimates*, Numer. Math., **41** (1983), pp. 39–53.

[39] M. Vogelius, *A right-inverse for the divergence operator in spaces of piecewise polynomials. Application to the p-version of the finite element method*, Numer. Math., **41** (1983), pp. 19–37.

[40] S. Zhang, *A new family of stable mixed finite elements for the 3d Stokes equations*, Math. Comp., **74** (2005), no. 250, pp. 543–554.

[41] S. Zhang, *Quadratic divergence-free finite elements on Powell-Sabin tetrahedral grids*, Calcolo, (2011), DOI: 10.1007/s10092-010-0035-4.